Nanoscale

Accepted Manuscript

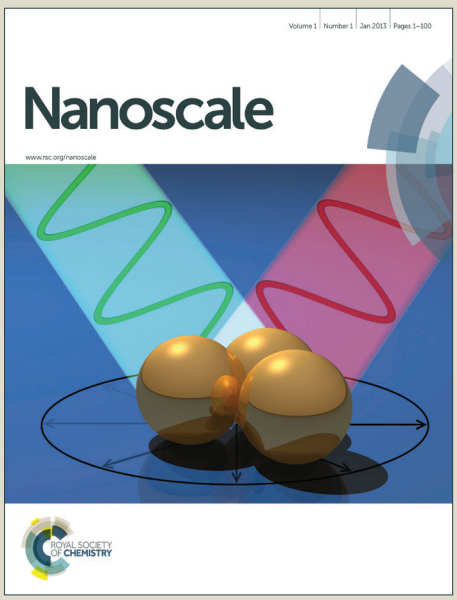

ROYAL SOCIETY OF CHEMISTRY

www.rsc.org/nanoscale

ARTICLE TYPE www. rsc.org/xxxxxx | XXXXXXXX

Surface Dangling Bonds Are a Cause of B-Type Blinking in Si Nanoparticles†

Nicholas P. Brawand,[ab] Márton Vörös [ab] and Giulia Galli[a*]

Received Xth XXXXXXXXXX 20XX, Accepted Xth XXXXXXXXX 20XX
First published on the web Xth XXXXXXXXXX 200X
DOI: 10.1039/b000000x

Exponential blinking statistics was reported in oxidized Si nanoparticles and the switching mechanism was attributed to the activation and deactivation of unidentified nonradiative recombination centers. Using ab initio calculations we predicted that Si dangling bonds at the surface of oxidized nanoparticles introduce defect states which, depending on their charge and local stress conditions, may give rise to ON and OFF states responsible for exponential blinking statistics. Our results are based on first principles calculations of charge transition levels, single particle energies, and radiative and nonradiative lifetimes of dangling bond defects at the surface of oxidized silicon nanoparticles under stress.

1 Introduction

Fluorescence intermittency, also known as blinking, refers to the stochastic switching between bright (ON) and dark (OFF) states of molecular emitters under continuous excitation and can be found in a wide variety of systems, from single violamine molecules[1] to semiconductor nanoparticles (NPs).[2] Blinking may be a detrimental effect which decreases the quantum efficiency, brightness and overall performance of NPs in several applications such as single-molecule imaging, lasers and NP solar cells. Blinking of individual NPs was first reported in CdSe two decades ago and it has since been observed in CdS, CdTe, ZnS and Si.[2–9] It is now believed that two types of blinking processes exist.[10] One, referred to as "A-type", is caused by photo-assisted Auger ionization. In the OFF state, all excited electron-hole (e-h) pairs recombine through nonradiative Auger recombination. The probabilities of the ON and OFF blinking times (t) follow a power law of the form $P(t) \propto t^{-\alpha}$ where $1 < \alpha < 2$ and several theoretical microscopic models were proposed to explain the switching mechanism.[7,8,11–17] We note that the power law distribution is ubiquitous in nature: earthquake magnitudes, solar flare intensities, wildfires sizes, the sizes of neuronal and sandpile avalanches all have a power law dependence and the origin of such dependence has been explained by the influential theory of self-organized criticality.[18,19]

Another type of blinking, B-type, is believed to be caused by the charging and discharging of yet unidentified, electron-accepting, nonradiative, recombination centers at the surface of the NPs.[10] For example, blinking was observed in Si/SiO_2 nanocrystals, and it was suggested that the "simple opening and closing of an efficient nonradiative recombination center" could be a reasonable explanation for the observed linear dependence of the blinking frequency on excitation power; however the nonradiative center has remained so far unidentified.[3,4,20] Indeed, several types of native defects exist at the Si/SiO_2 interface and it is yet unclear which of them may cause blinking in $NPSi/SiO_2$ systems.[21–24]

One of the most common defects at the Si/SiO_2 interface, both in the bulk and in NPs, is the silicon dangling bond (DB), which has been the focus of several theoretical and experimental investigations.[25–39] At the bulk Si interface the isolated DB can exist in three different charge states: negative D^-, neutral D^0 and positive D^+ with two electronic transitions positioned 0.3 eV above the VBM and 0.25 eV below the CBM, respectively.[40,41] After oxidation, the density of DB defects on a bulk Si surface may be of the order of 10^{12} cm^{-2} and even at these densities, DBs may be detrimental to the functionality of electronic devices.[33,42] Though bulk silicon-silicon-oxide interfaces have been extensively studied, given their interest to the electronics industry, much less is known about the properties of DB defects on the surface of oxidized Si NPs.

In particular, all first principle studies of DBs at the surface of Si NPs were so far focused on hydrogen terminated samples in the absence of a host matrix[43,44], which is however known to influence the electronic properties of the NPs.[45,46] It is now known that quantum confinement leads to Si DB charge transition levels (CTLs) which are asymmetrically positioned within the electronic gap of fully hydrogen passivated Si NPs. Neutral DBs at the surface of hydrogenated Si NPs were predicted to be efficient nonradiative recombination centers responsible

† Electronic Supplementary Information (ESI) available: bulk defect structure geometry, decay dynamics and estimation of crossing region. See DOI: 10.1039/b000000x/

[a] *The University of Chicago, Chicago, United States. Fax: 773 795 9106; Tel: +1 773 702 0515; E-mail: gagalli@uchicago.edu*
[b] *The University of California, Davis, United States.*

for low electron mobilities in organic-inorganic hybrid nanostructure materials[44]; recombination on charged DBs was instead found to be a radiative process for small Si crystallites with gap energies higher than 2.2 eV, at low temperatures.[47]

In this work, we used ab initio calculations to investigate the electronic properties and charge recombination dynamics in oxidized Si NPs containing surface DBs. We focused on the relative probability of radiative and nonradiative recombination processes[48–51] as a function of stress at or close to the surface of the NP, where defects are present. From our results, we predicted that surface DBs introduce defect states which can cause blinking within oxidized Si NPs, and these DB states are responsible for the exponential blinking statistics observed experimentally in Si NP/oxide composites. Our study is the first to report ab initio calculations of recombination rates of defects at oxidized Si NP surfaces.

2 Structural Models

We considered three Si NPs; $Si_{77}O_{52}H_{76}$, $Si_{116}O_{72}H_{84}$ and $Si_{238}O_{119}H_{132}$ terminated with one oxidized layer, with diameters of 1.3, 1.6 and 1.9 nm respectively. These NPs were obtained in a previous study[46] through a coupled classical-ab initio molecular dynamics (MD) approach, by annealing Si NPs within an amorphous SiO_2 matrix consisting of 648 atoms.

After annealing, the NPs and their interfacial oxide layer shells were extracted from the host matrix and terminated by hydrogen atoms, so as to saturate all dangling bonds of the oxide. The projected density of states of the embedded and extracted NPs were compared, and found to be almost identical. We hence considered the extracted NPs with an oxide layer as representative of a Si NP under the stress conditions exerted by the matrix and, for computational simplicity, we studied the electronic properties of defects in the extracted NPs.

At the surface of the latter, we introduced three different types of DB defects, traditionally denoted: P_b, P_{b1} and P_{b0}, * and we optimized the positions of nearest neighbor atoms under three different conditions, mimicking the presence of different stress fields on the surface of the nanoparticles. First, we simulated the presence of a highly constrained environment where only atoms that are nearest neighbors of the defect are allowed to relax (we denote this configuration by r_{nn}). We then considered the conditions under which only the outer most layer was held fixed and the interior atoms, including nearest neighbors of the defect, were allowed to relax (configuration r_{np}). Finally, we simulated a free standing NP where all atoms were allowed to relax (configuration r_∞). The final geometry of the smallest extracted model without any relaxation is presented in Figure 1.

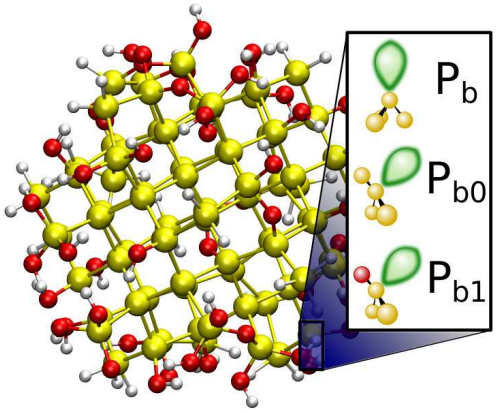

Fig. 1 Model of a 1.3 nm silicon nanoparticle terminated by an oxide layer, as extracted from an amorphous matrix of SiO_2 (see text). The three dangling bond defect geometries studied in this work, labeled P_b, P_{b0} and P_{b1}, are shown.[31,52] The P_b defect, originally found at the (111) interface of bulk Si/SiO_2 is back-bonded to three Si atoms. The P_{b0} and P_{b1} are both at the (100) interface. The P_{b0} is back-bonded to three Si atoms, while P_{b1} is back-bonded to two Si and one O atoms. The P_{b1} defect has been modeled using the geometry proposed by Poindexter et al.[31] Silicon, oxygen and hydrogen atoms are represented by yellow, red and white spheres, respectively. Each nanoparticle modeled in this work has a maximum of one dangling bond defect.

3 Theory and Computational Methods

Usually, the presence of DBs introduce electronic defect states within the energy gap of the host semiconductor. Such states may become charged through different mechanisms, including (i) the exchange of electrons or holes with surrounding defects within the host matrix, (ii) the variation of the Fermi level by applying an electric field, or (iii) a change in the doping levels within the sample.

In order to study charge defects and compare their relative stability, it is useful to define charge transition levels. The value of the Fermi level ($\varepsilon(q_1/q_2)$) at which two charge states, q_1 and q_2, of the same defect have the same formation energy is called the charge transition level and is defined as:

$$\varepsilon(q_1/q_2) = \frac{E^f(X^{q_1};E_F=0) - E^f(X^{q_2};E_F=0)}{q_2 - q_1} \quad (1)$$

* The DB defect geometries are labeled P_b, P_{b0} and P_{b1} to indicate that the defects are Paramagnetic; they were first reported in Ref. 52. The P_b defect is found at the bulk $Si(111)/SiO_2$ interface while the P_{b1} and P_{b0} have been reported to exist at the $Si(100)/SiO_2$ interface.[31]

where E_F is the Fermi level and $E^f(X^{q_1};E_F=0)$ is the formation energy of defect X in charge state q_1.[53] In our calculations of E^f, atomic positions were allowed to relax within specific relaxation conditions (r_{nn} or r_∞), hence the transition levels reported in this work correspond to thermodynamic transition levels, as defined in Ref. 54.

To compute the nonradiative capture rates by a single DB we need to calculate the transition rate from a thermalized state manifold given by[55]:

$$k_{nr} = \sum_m f_m k_m \tag{2}$$

where m is the initial vibrational state manifold index, f_m is the quantum statistical equilibrium distribution and k_m is the transition rate of state m. In this work we treated the interaction to first order in the electron-phonon coupling and because the initial state is expected to decay to a manifold of final vibrational states, we may replace k_m in Equation 2 with Fermi's golden rule. Furthermore, we assumed the nonradiative transition processes to take place between two electronic states, along a single effective reaction coordinate, with both states characterized by the same single vibrational frequency ω. The path of the effective parabolic vibrational mode was defined by $\{R_x\} = x\{R_f\} + (1-x)\{R_i\}$, where $\{R_i\}$ and $\{R_f\}$ are the optimized atomic coordinates of the system in the initial and final electronic states, respectively, as x is varied from 0 to 1. Under these conditions, Equation 2 gives the full quantum (FQ) transition rate:

$$k_{nr}^{FQ} = \sum_{m,n} f_m \frac{2\pi}{\hbar} |v|^2 |\langle \chi_{im}|Q-Q_i|\chi_{fn}\rangle|^2 \delta\left(E_o + m\hbar\omega - n\hbar\omega\right) \tag{3}$$

where E_o is the ionization energy of the defect defined as $E_o = E_i(\{R_i\}) - E_f(\{R_f\})$, $\chi_{i,m}$ is the harmonic wavefunction of the effective vibrational state with quantum number m, when the electron is in state i; $Q-Q_i$ is the difference between the configuration coordinate of the reaction and the equilibrium configuration coordinate corresponding to an electron in the initial state i defined by $Q-Q_i = \Sigma_j \sqrt{M_j}(R_j - R_{i,j})$, where M_j is the mass of the j^{th} atom, R_j is the position of the j^{th} atom and $R_{i,j}$ is the equilibrium position of the j^{th} atom when the electron is in the initial state. f_m is the Bose-Einstein occupation of the vibrational state m and v is the electronic coupling computed within the static and linear coupling approximations[48,49]:

$$v = (\varepsilon_f - \varepsilon_i)\langle \psi_i(r;\{R_i\})|\frac{\partial \psi_f(r;\{R_i\})}{\partial Q}\rangle \tag{4}$$

where we assumed the many body electronic wavefunctions can be replaced by the single particle Kohn-Sham orbitals $\psi_i(r;\{R_i\})$ and $\psi_f(r;\{R_i\})$, i.e. the eigenfunctions of the electronic Hamiltonian at $\{R_i\}$; ε_i and ε_f are the respective eigenvalues.

In the high temperature limit $\hbar\omega \ll k_bT$ the ions can be treated classically and $f_m \approx \frac{\hbar\omega}{k_bT} e^{-\beta(E-E_i(\{R_i\}))}$, where $\beta = (k_bT)^{-1}$. Furthermore if v is small then k_m in Equation 2 can be replaced with $\frac{\omega}{\pi} P_{i\to f}$ where $P_{i\to f}$ is the probability that a transition $\psi_i \to \psi_f$ occurs, given by the Landau-Zener formula.[56] Under these conditions and making the substitution $\sum_m \to \int \frac{dE}{\hbar\omega}$, Equation 2 simplifies to the well known Marcus theory equation:[48,57]

$$k_{nr}^{Marcus} = |V|^2 \sqrt{\frac{\pi\beta}{\hbar^2 E_{FC}}} e^{-\beta E_{act}} \tag{5}$$

where E_{FC} is the Franck-Condon shift and $V = v(Q-Q_i)$, when $Q-Q_i$ is evaluated at the crossing point. E_{act} is the activation energy given by:

$$E_{act} = \frac{(E_o - E_{FC})^2}{4E_{FC}}, \tag{6}$$

If we treat both the ions and the electron classically, then k_m can be replaced by $\frac{\omega}{\pi}\Theta(E-E_{act})$ so that the probability of the electron transition occurring is 1 if the energy of the system is greater than the activation energy. Under these conditions, Equation 2 gives the classical transition rate:

$$k_{nr}^{C} = \frac{\omega}{\pi} e^{-\beta E_{act}} \tag{7}$$

Equations 3, 5 and 7 serve as the basis for all nonradiative transition rate calculations considered in this work.

Radiative recombination rates were estimated using Fermi's golden rule and the dipole approximation and they are given by[58,59]:

$$k_r = \frac{4n\alpha\omega^3}{3c^2} |\langle \psi_i(r;\{R_i\})|\mathbf{r}|\psi_f(r;\{R_i\})\rangle|^2 \tag{8}$$

where $\hbar$ has been set to 1, c is the speed of light in vacuum and ω is the transition energy. Because the NP is mostly composed of Si atoms and we are only interested in the comparison of k_r and k_{nr} which, according to our results, differ by more than two orders of magnitude, the index of refraction (n) was approximated by that of bulk Si. We checked the strain dependence of the radiative lifetimes by calculating the decay rates of an excited electron in the fully relaxed and strained 1.3 nm NPs. We found both rates to be of the order of 10^6 s^{-1}, which is within the same order of magnitude of other theoretical predictions.[60,61]

Geometry optimizations and all other results reported in this work were obtained using density functional theory (DFT) as implemented in the software package Quantum Espresso[62]. The generalized gradient corrected PBE functional[63] was used

as an approximation for the exchange and correlation energy. Norm-conserving Rappe Rabe Kaxiras Joannopoulos (RRKJ)[64] pseudopotentials in separable (Kleinman-Bylander) form from the Quantum Espresso library[62] were adopted to describe the effective interaction between valence electrons and frozen ionic cores. The single particle Kohn-Sham (KS) orbitals were represented using a plane wave basis with a maximum energy cutoff of 80 Rydberg; energies and wavefunctions were considered converged after the estimated error on the electronic total energy was less than 10^{-8} Ry. Geometry optimizations were considered converged if all forces were less than 10^{-3} Ry/Bohr. Total energies of charged systems were obtained using the Makov-Payne correction (MPC) scheme.[65]

4 Results and Discussion

In the following we discuss our results for the electronic properties of the neutral and charged dangling bond defects and for several radiative and nonradiative decay processes. By comparing computed values of k_r and k_{nr} as a function of the local stress in the NP, we show that decay channels are strongly dependent on strain and hence on the effect of the matrix on the NP. Finally we discuss blinking and its dependence on strain.

We first discuss our calculations of thermodynamic charge transition levels showing that the levels of P_b, P_{b1} and P_{b0} are stress dependent. The computed charge transition levels for the P_b, P_{b1} and P_{b0} defects on the surface of strained, oxidized 1.3 nm Si NPs are presented in Figure 2. They were obtained as total energy differences using Equation 1. All calculations represented by solid lines were carried out in the configuration characterized by the coordinate r_{nn}.

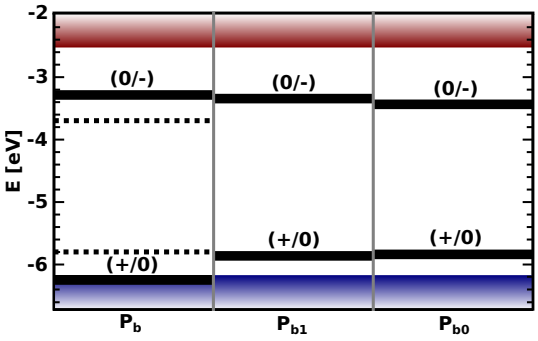

Fig. 2 Charge transition levels for the P_b, P_{b1} and P_{b0} defects on the surface of strained oxidized 1.3 nm silicon NPs. The lowest and uppermost positions of the blue and red areas represent the negative of the ionization potential and electron affinity of the defectless oxidized 1.3 nm nanoparticle, respectively. Dashed lines are the charge transition levels computed for the same NP but in the absence of stress. The energy levels are all referenced to vacuum.

The dashed lines represent the CTLs of the fully relaxed NP with a single P_b defect in an unstrained configuration; the comparison with the solid line for the same system highlights the effect of strain in determining the CTLs. In agreement with Ref. 43, we found that the CTL of the P_b defect is asymmetrically positioned within the gap of the defectless NP. This asymmetry is also present in the case of the P_{b1} and P_{b0} defects. Assuming the Fermi level can lie anywhere within the gap of the NP, then Figure 2 shows that the most likely charge state of the NP is the neutral charge state. Therefore, we now turn our attention to the single particle energy levels of the NP with a neutral DB defect, and verify that the defect states remain within the NP gap as its diameter is varied.

It is well known that DFT underestimates energy gaps, but it has nevertheless proven to be a useful tool to predict *trends* of energy gaps, e.g. as a function of NP size. In Figure 3 we present the HOMO/LUMO gaps of two DB defect geometries as a function of NP size. Not shown in Figure 3 are the P_{b0} gaps which were found to differ from those of the P_b defect by less than 0.05 eVs for the smallest NP. Our results predict that the defect energy levels remain within the gap of the oxidized NPs for all diameters.

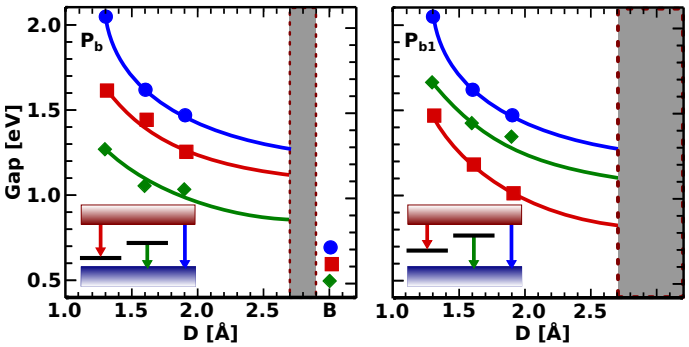

Fig. 3 HOMO/LUMO gaps of the P_b and P_{b1} surface defect states in the presence of a strained oxide layer on the surface of three different Si nanoparticles. The insets represent the single particle energy levels and the corresponding gaps given by the colored arrows.

The bulk model, "B" reported Figure 3, was simulated by a 215 Si atom supercell with a single dangling bond defect at the center. The neighboring atoms around the defect were passivated using an oxygen bridge and a hydrogen atom. A complete description of the bulk model is provided in the supplementary material.

Having established that the single particle energy levels associated with the stable neutral defect are in the gap of the NPs, we now focus on the P_b defect on the surface of the 1.3 nm oxidized NP. We first discuss the potential energy surfaces corresponding to the electronic excitations displayed in Figure 3. Though the full PESs are not required to calculate k_{nr},

they help to visualize the decay processes. A qualitative description of the configuration coordinate is provided in Ref. 40. The PESs were obtained by fitting parabolas to the total energy calculations required to obtain E_o and E_{FC} for the P_b defect on the surface of the 1.3 nm NP, within the r_{nn} relaxation condition. Two spin channels can be excited as shown in the two panels of Figure 4.

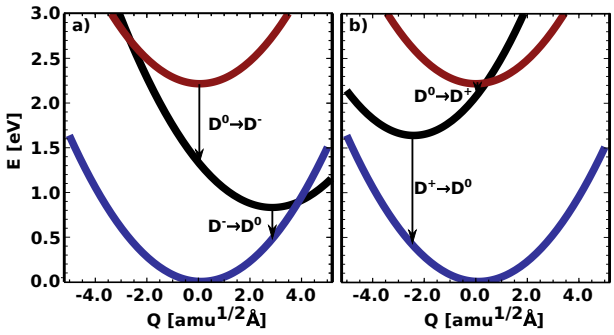

Fig. 4 Configuration coordinate diagrams for the decay processes belonging to two separate spin channels. The notation $D^{\alpha} \rightarrow D^{\beta}$ denotes the transition of the dangling bond from charge state α to charge state β. See text for further description.

Though several atoms move along different paths during each of the reactions depicted in Figure 4, the configuration coordinate on the x-axis of Figure 4 represents, on average, the position of a three-fold coordinated silicon surface atom along a radial direction of the NP, with the origin corresponding to the equilibrium position of the atom, and with the DB in the neutral charge state (D^0). The red curve corresponds to the DB in the neutral charge state (D^0) with an excited carrier in the conduction band. As the system relaxes the charge state of the DB changes. Depending on which spin channel the excited carrier occupies, the DB may transition to either the negative (D^-) or positive (D^+) charge state represented by the black curves in panels a) and b), respectively. During the transition from (D^0) to (D^-), the three-fold coordinated atom moves away from its nearest neighbors at equilibrium and from the NP center, in the positive radial direction. During the transition from (D^0) to (D^+), the three-fold coordinated surface atom moves in the negative radial direction towards the plane formed by its three nearest neighbors. When relaxation is completed, the DB returns to the neutral charge state (D^0).

The PESs of Figure 4 show that the nonradiative $D^+ \rightarrow D^0$ decay process is much slower than the other processes shown in Figure 4. However, the PESs may vary, depending on the amount of strain induced by the surrounding matrix. To elucidate the effect of strain on the character of recombination processes, we plotted in Figure 5 the $\ln(k_r/k_{nr})$ for the four decay processes outlined in Figure 4, as a function of decreasing strain.

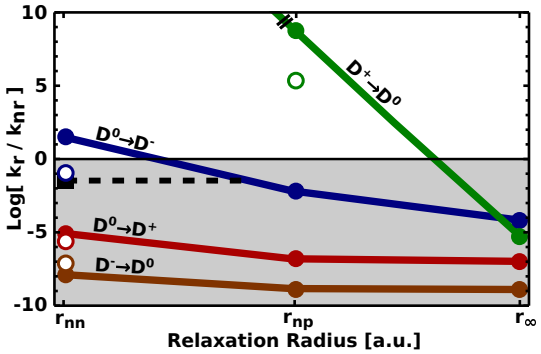

Fig. 5 The logarithm of the ratio between radiative (k_r) and nonradiative (k_{nr}) decay rates for the four capture processes outlined in Figure 4, as a function of decreasing strain on the NP (see text), for a P_b defect at the surface of a 1.3 nm Si NP terminated by an oxide layer. The black horizontal line represents the boundary between radiative (white area) and nonradiative (gray area) recombination processes. Configurations representing different relaxation schemes around the defect (and hence different amount of strain) are shown on the x axis: r_{nn} (nearest neighbor), r_{np} (Si NP and first layer of oxygen) and r_{∞} (all atoms in the system). Nonradiative rates given by Equation 7 and 3 are indicated by the dots and open circles respectively.

Nonradiative recombination rates for the processes displayed in Figure 4 and the r_{nn} configurations were also calculated using Marcus theory (Equation 5). After comparing the two methods, Equations 5 and 7, we found the characters (radiative or nonradiative) of all the transitions within the r_{nn} configuration to be unchanged.

It is clear from Figure 5, that the nonradiative recombination rates are highly sensitive to the number of atoms that are permitted to relax around the defect, due to the exponential dependence of k_{nr} on E_{act}. The largest k_{nr}^{FQ} is of the order of $10^{12}s^{-1}$ which is the same order of magnitude as that predicted by H. Li, et al. for the charge recombination rate at a $Si_{147}H_{100}$/P3HT interface in the presence of a dangling bond.[44] The nonradiative recombination rates were calculated for the three different configurations defined earlier (r_{nn}, r_{np} and r_{∞}). By holding some atoms fixed during relaxation we preserved the strain induced by the original surrounding matrix. Calculations allowing only nearest neighbor atoms to relax (r_{nn}) simulate a system where the matrix has a strong effect on the surface strain of the NP. Instead, the r_{∞} calculations simulate a free standing NP in the absence of the stress exerted by a host matrix. Our results show that the amount of strain – which was shown to be dependent on the density of the matrix and the size of the NP[46] – is a key factor in determining whether a recombination channel is radiative or nonradiative. For example, the $D^0 \rightarrow D^-$ process is predicted to be radiative in the r_{nn} configurations; however, the same process

is predicted to be nonradiative for configuration r_{np}. Overall we found that the strain caused by the matrix increases the nonradiative recombination lifetimes with respect to that of unstrained NPs.

We also built an additional model of the P_b defect at a different location on the NP, indicated by the square in Figure 5. The qualitative behavior (whether a channel is radiative or nonradiative) of this model agrees with that reported in Figure 5 by the dots, except for the $D^0 \rightarrow D^-$ process which is predicted to be nonradiative for the r_{nn} geometry.

The nonradiative recombination rates also depend on the size of the NP, mostly through the dependence of the ionization energy on quantum confinement. As the size of the NP increases, the confinement energy decreases causing E_o to approach E_{FC} and thus decreasing the energy barrier (see Equation 6). While nonradiative recombination becomes more efficient as the size of the NP becomes larger, we expect the opposite trend for the radiative transitions, due to a reduction of the overlap between the HOMO/LUMO and the DB state, as well as the decrease in the energies of the transitions.[60] Hence, we predict there will be a crossing region where the $D^+ \rightarrow D^0$ process will become nonradiative. If we assume E_{FC} and k_r to be size independent, we predict that the $D^+ \rightarrow D^0$ process will become nonradiative for NPs larger than about 4 nm in diameter. Quasi-particle corrections to DFT single particle energies nearly cancel the exciton binding energy in Si NPs[66]; hence the values of computed DFT gaps are representative of measured optical gaps. In terms of quasi-particle gaps our calculations are representative of NPs with larger radii.

Because the nonradiative lifetimes of the $D^+ \rightarrow D^0$ process is several orders of magnitude larger than the corresponding radiative one, if strain is present for both *Pb* models, we predict that the capture of an electron by a positively charged DB on the surface of an oxidized NP is most likely a radiative process for NPs smaller than about 4 nm in diameter. Instead, $D^- \rightarrow D^0$ is most likely nonradiative. These results differ from previous results obtained from empirical tight binding theory for hydrogen passivated NCs, which predicted both $D^- \rightarrow D^0$ and $D^+ \rightarrow D^0$ to be radiative processes.[47]

5 Analysis of Blinking Processes

Our calculations showed that there are strain conditions, represented by the coordinates r_{np} that, in the presence of DBs, may give rise to ON and OFF states in small oxidized Si nanocrystals. If a NP with a DB is excited while in the negatively charged state, the fastest recombination channels are all nonradiative, resulting in the OFF state. If the system is excited while in the positively or neutrally charged state, half of the recombination channels are radiative for both states but only the positively charged state is likely to emit photons with energies equal to the intrinsic gap of the NP. Hence, we label the positive charge state ON and the neutral state OFF. Therefore, the charge state of the DB can determine if the NP is in the ON or OFF state. A summary of the decay dynamics is provided in the supplementary material.

Switching between the OFF and ON state can occur if an electron from a neutral NP with a surface DB were to tunnel to the several possible defects that exist in the surrounding oxide.[21] Doing so would cause the NP/DB system to become positively charged (ON) until an electron transfer returns the system back to the neutral charge state (OFF). Hence our calculations provide an explanation for blinking processes observed in Si NPs.[3–5,9,67,68] We note that recent experiments detecting blinking processes have been interpreted in terms of nonradiaitve recombination centers inside of or near CdSe/CdS/ZnS/InP NPs[14,15] and Si NPs,[3,4,9] where the switching frequency between ON and OFF states was found to depend linearly on the input power. This property suggests that the switching mechanism may indeed depend on single excitation processes, as our calculations suggest, rather than on more complex processes such as Auger recombination.

6 Conclusion

Using ab initio calculations within density functional theory, we investigated the charge transition levels and recombination rates in Si NPs with oxidized surface layers and DB defects present at the surface. We showed that, depending on the charge state and strain conditions at the surface, DBs may act as nonradiative recombination centers. Based on these results, we predicted that surface dangling bonds introduce defect states at the surface of oxidized Si NPs that can cause ON and OFF blinking states. Switching between ON and OFF could be caused by charge transfer to other local defects or by temporary passivation of the DB state.

Hence our work provided a microscopic picture to explain how blinking may be achieved through surface DBs, which are highly sensitive to the local strain around each NP; however, as previously mentioned, blinking may also occur by photo-assisted Auger ionization. The coexistence of multiple mechanisms, with one being highly sensitive to strain, may explain the observed variation in the type of blinking exhibited by different NPs within the same sample.[4] Our results indicate that in a given sample, the number of NPs exhibiting exponential type blinking varies with size, strain and surface passivation. Hydrogen treatment[69–71] and annealing[71–73] may help reduce the density of dangling bands possibly reducing the amount of blinking. Deep level transient spectroscopy could be used to quantify the effects of strain by measuring charge transition levels and electron spin resonance experiments would be a good additional probe to validate our predictions.

Our results are the first reported ab initio calculations showing that dangling bonds on the surface of oxidized Si NPs can

act as efficient nonradiative recombination centers or traps. Our findings thus also provide an *a priori* validation of the interpretation of the role that dangling bond defects play in several photonic and optoelectronic devices.[74–78]

Acknowledgement

The authors would like to thank Tianshu Li, Tingyi Gu, Kenton T. Seward, T. Anh Pham, Audrius Alkauskas, Gergely Zimanyi and Alex P. Gaiduk for informative discussions. This work was supported by the Department of Energy/Basic Energy Sciences grant No. DE-FG02-06ER46262. This research used resources of the National Energy Research Scientific Computing Center (NERSC) through the NISE project Larnint. NERSC is supported by the Office of Science of the U.S. Department of Energy under Contract No. DE-AC02-05CH11231.

References

1 E. A. Riley, C. Bingham, E. D. Bott, B. Kahr and P. J. Reid, *Phys. Chem. Chem. Phys.*, 2011, **13**, 1879–1887.
2 M. Nirmal, B. O. Dabbousi, M. G. Bawendi, J. J. Macklin, J. K. Trautman, T. D. Harris and L. E. Brus, *Nature*, 1996, **383**, 802–804.
3 B. Bruhn, F. Qejvanaj, I. Sychugov and J. Linnros, *J. Phys. Chem. C*, 2014, **118**, 2202–2208.
4 B. Bruhn, J. Valenta, F. Sangghaleh and J. Linnros, *Nano Lett.*, 2011, **11**, 5574–5580.
5 F. Cichos, J. Martin and C. von Borczyskowski, *Phys. Rev. B*, 2004, **70**, 115314.
6 R. G. Neuhauser, K. T. Shimizu, W. K. Woo, S. A. Empedocles and M. G. Bawendi, *Phys. Rev. Lett.*, 2000, **85**, 3301.
7 R. Verberk, A. M. van Oijen and M. Orrit, *Phys. Rev. B*, 2002, **66**, 233202.
8 K. T. Shimizu, R. G. Neuhauser, C. A. Leatherdale, S. A. Empedocles, W. K. Woo and M. G. Bawendi, *Phys. Rev. B*, 2001, **63**, 205316.
9 B. Bruhn, F. Qejvanaj, T. Gregorkiewicz and J. Linnros, *Physica B*, 2014, **453**, 63 – 67.
10 C. Galland, Y. Ghosh, A. Steinbrück, M. Sykora, J. A. Hollingsworth, V. I. Klimov and H. Htoon, *Nature*, 2011, **479**, 203–207.
11 A. L. Efros and M. Rosen, *Phys. Rev. Lett.*, 1997, **78**, 1110.
12 J. Tang and R. A. Marcus, *J. Chem. Phys*, 2005, **123**, 1–12.
13 M. Kuno, D. P. Fromm, S. T. Johnson, A. Gallagher and D. J. Nesbitt, *Phys. Rev. B*, 2003, **67**, 125304.
14 S. Rosen, O. Schwartz and D. Oron, *Phys. Rev. Lett.*, 2010, **104**, 157404.
15 M.-E. Pistol, P. Castrillo, D. Hessman, J. A. Prieto and L. Samuelson, *Phys. Rev. B*, 1999, **59**, 10725.
16 O. Voznyy and E. H. Sargent, *Phys. Rev. Lett.*, 2014, **112**, 157401.
17 F. M. Gómez-Campos and M. Califano, *Nano Lett.*, 2012, **12**, 4508–4517.
18 P. Bak, C. Tang and K. Wiesenfeld, *Phys. Rev. Lett.*, 1987, **59**, 381.
19 D. Markovi and C. Gros, *Phys. Rep.*, 2014, **536**, 41 – 74.
20 B. Bruhn, F. Sangghaleh and J. Linnros, *Phys. Status Solidi A*, 2011, **208**, 631–634.
21 A. Alkauskas, P. Broqvist and A. Pasquarello, *AIP Conf. Proc.*, 2010, **1199**, 79–80.
22 Y. Shu and B. G. Levine, *The Journal of Physical Chemistry C*, 2014, **118**, 7669–7677.
23 E. P. O'Reilly and J. Robertson, *Phys. Rev. B*, 1983, **27**, 3780.
24 G. Pacchioni, L. Skuja and D. Griscom, *Defects in SiO_2 and Related Dielectrics: Science and Technology*, Springer Netherlands, 2000.
25 R. N. Pereira, D. J. Rowe, R. J. Anthony and U. Kortshagen, *Phys. Rev. B*, 2011, **83**, 155327.
26 E. H. Poindexter and P. J. Caplan, *Prog. Surf. Sci.*, 1983, **14**, 201 – 294.
27 E. H. Poindexter, P. J. Caplan, B. E. Deal and R. R. Razouk, *J. Appl. Phys*, 1981, **52**, 879–884.
28 A. Stesmans, *Phys. Rev. Lett.*, 1993, **70**, 1723.
29 E. H. Poindexter, G. J. Gerardi, M. Rueckel, P. J. Caplan, N. M. Johnson and D. K. Biegelsen, *J. Appl. Phys*, 1984, **56**, 2844–2849.
30 V. Y. Bratus, V. A. Yukhimchuk, L. I. Berezhinsky, M. Y. Valakh, I. P. Vorona, I. Z. Indutnyi, T. T. Petrenko, P. E. Shepeliavyi and I. B. Yanchuk, *Semiconductors*, 2001, **35**, 821–826.
31 E. H. Poindexter, P. J. Caplan, B. E. Deal and R. R. Razouk, *J. Appl. Phys*, 1981, **52**, 879–884.
32 A. Stesmans, B. Nouwen and V. V. Afanas'ev, *Phys. Rev. B*, 1998, **58**, 15801.
33 K. Keunen, A. Stesmans and V. V. Afanas'ev, *Phys. Rev. B*, 2011, **84**, 085329.
34 T. Matsuoka, L. S. Vlasenko, M. P. Vlasenko, T. Sekiguchi and K. M. Itoh, *Appl. Phys. Lett.*, 2012, **100**, 1–3.
35 H. Kageshima and K. Shiraishi, *Surf. Sci.*, 1997, **380**, 61 – 65.
36 H. Kageshima and K. Shiraishi, *Surf. Sci.*, 1998, **407**, 133 – 139.
37 J. R. Weber, A. Janotti and C. G. Van de Walle, *Phys. Rev. B*, 2013, **87**, 035203.
38 M. Hane, Y. Miyamoto and A. Oshiyama, *Phys. Rev. B*, 1990, **41**, 12637.

39 M. Beltrán, *J. Non-Cryst. Solids*, 1993, **163**, 148 – 161.

40 C. Delerue and M. Lannoo, *Nanostructures: Theory and Modeling*, Springer, Verlag Berlin Heidelberg, 2004.

41 N. M. Johnson, D. K. Biegelsen, M. D. Moyer, S. T. Chang, E. H. Poindexter and P. J. Caplan, *Appl. Phys. Lett.*, 1983, **43**, 563–565.

42 A. H. Edwards, *Phys. Rev. B*, 1991, **44**, 1832.

43 K.-H. Hong, J. Kim, J. H. Lee, J. Shin and U.-I. Chung, *Nano Lett.*, 2010, **10**, 1671–1676.

44 H. Li, Z. Wu and M. T. Lusk, *J. Phys. Chem. C*, 2014, **118**, 46–53.

45 R. Guerra and S. Ossicini, *Phys. Rev. B*, 2013, **87**, 165441.

46 T. Li, F. Gygi and G. Galli, *Phys. Rev. Lett.*, 2011, **107**, 206805.

47 M. Lannoo, C. Delerue and G. Allan, *J. Lumin*, 1993, **57**, 243 – 247.

48 P. T. Landsberg, *Recombination in Semiconductors*, Cambridge University Press, NY, USA, 1991, p. 462.

49 A. Alkauskas, Q. Yan and C. G. Van de Walle, *Phys. Rev. B*, 2014, **90**, 075202.

50 Y. Shu and B. G. Levine, *J. Chem. Phys*, 2013, **139**, 1–4.

51 J. Liu, A. J. Neukirch and O. V. Prezhdo, *J. Phys. Chem. C*, 2014, **118**, 20702–20709.

52 Y. Nishi, *Jpn. J. Appl. Phys*, 1971, **10**, 52–62.

53 C. Freysoldt, B. Grabowski, T. Hickel, J. Neugebauer, G. Kresse, A. Janotti and C. G. Van de Walle, *Rev. Mod. Phys.*, 2014, **86**, 253–305.

54 C. Freysoldt, B. Grabowski, T. Hickel, J. Neugebauer, G. Kresse, A. Janotti and C. G. Van de Walle, *Rev. Mod. Phys.*, 2014, **86**, 253–305.

55 V. May and O. Kuhn, *Charge and Energy Transfer Dynamics in Molecular Systems*, Wiley-VCH, Weinheim, Germany, 2011.

56 C. Zener, *Proc. Roy. Soc. A*, 1932, **137**, 696.

57 R. A. Marcus, *Faraday Discuss. Chem. Soc.*, 1982, **74**, 7–15.

58 M. Califano, A. Franceschetti and A. Zunger, *Phys. Rev. B*, 2007, **75**, 115401.

59 L. D. Dal Negro, J. H. Yi, J. Michel, L. C. Kimerling, S. Hamel, A. Williamson and G. Galli, *IEEE J. Quant. Electron*, 2006, **12**, 1628–1635.

60 R. Guerra and S. Ossicini, *Phys. Rev. B*, 2010, **81**, 245307.

61 X. Chen, X. Pi and D. Yang, *J. Phys. Chem. C*, 2010, **114**, 8774–8781.

62 P. Giannozzi, S. Baroni, N. Bonini, M. Calandra, R. Car, C. Cavazzoni, D. Ceresoli, G. L. Chiarotti, M. Cococcioni, I. Dabo, A. D. Corso, S. de Gironcoli, S. Fabris, G. Fratesi, R. Gebauer, U. Gerstmann, C. Gougoussis, A. Kokalj, M. Lazzeri, L. Martin-Samos, N. Marzari, F. Mauri, R. Mazzarello, S. Paolini, A. Pasquarello, L. Paulatto, C. Sbraccia, S. Scandolo, G. Sclauzero, A. P. Seitsonen, A. Smogunov, P. Umari and R. M. Wentzcovitch, *J. Phys: Condens. Matter*, 2009, **21**, 395502–395521.

63 J. P. Perdew, K. Burke and M. Ernzerhof, *Phys. Rev. Lett.*, 1996, **77**, 3865.

64 A. M. Rappe, K. M. Rabe, E. Kaxiras and J. D. Joannopoulos, *Phys. Rev. B*, 1990, **41**, 1227.

65 G. Makov and M. C. Payne, *Phys. Rev. B*, 1995, **51**, 4014.

66 C. Delerue, M. Lannoo and G. Allan, *Phys. Rev. Lett.*, 2000, **84**, 2457–2460.

67 I. Sychugov, R. Juhasz, J. Linnros and J. Valenta, *Phys. Rev. B*, 2005, **71**, 115331.

68 J. Valenta, A. Fucikova, F. Vcha, F. Adamec, J. Humpolkov, M. Hof, I. Pelant, K. Ksov, K. Dohnalov and J. Linnros, *Adv. Funct. Mater*, 2008, **18**, 2666–2672.

69 R. N. Pereira, D. J. Rowe, R. J. Anthony and U. Kortshagen, *Phys. Rev. B*, 2012, **86**, 085449–085454.

70 B. G. Lee, D. Hiller, J.-W. Luo, O. E. Semonin, M. C. Beard, M. Zacharias and P. Stradins, *Advanced Functional Materials*, 2012, **22**, 3223–3232.

71 D. Hiller, S. Gutsch, A. M. Hartel, P. Lper, T. Gebel and M. Zacharias, *J. Appl. Phys.*, 2014, **115**, 134311–134319.

72 S. Niesar, R. N. Pereira, A. R. Stegner, N. Erhard, M. Hoeb, A. Baumer, H. Wiggers, M. S. Brandt and M. Stutzmann, *Adv. Funct. Mater*, 2012, **22**, 1190–1198.

73 S. Niesar, A. R. Stegner, R. N. Pereira, M. Hoeb, H. Wiggers, M. S. Brandt and M. Stutzmann, *Appl. Phys. Lett.*, 2010, **96**, 193112–193115.

74 A. R. Stegner, R. N. Pereira, K. Klein, R. Lechner, R. Dietmueller, M. S. Brandt, M. Stutzmann and H. Wiggers, *Phys. Rev. Lett.*, 2008, **100**, 026803–026807.

75 L. Pavesi and R. Turan, *Silicon Nanocrystals: Fundamentals, Synthesis and Applications*, Wiley, 2010.

76 M. Lopez, B. Garrido, C. Garca, P. Pellegrino, A. Prez-Rodrguez, J. R. Morante, C. Bonafos, M. Carrada and A. Claverie, *Appl. Phys. Lett.*, 2002, **80**, 1637–1639.

77 R. N. Pereira, S. Niesar, W. B. You, A. F. da Cunha, N. Erhard, A. R. Stegner, H. Wiggers, M. G. Willinger, M. Stutzmann and M. S. Brandt, *J. Phys. Chem. C*, 2011, **115**, 20120–20127.

78 S. Gutsch, J. Laube, A. M. Hartel, D. Hiller, N. Zakharov, P. Werner and M. Zacharias, *J. Appl. Phys.*, 2013, **113**, 133703–133712.